CFD Study on Propeller-Induced Pressure Pulses in Cavitating Flows

Keun Woo Shin[*] and Poul Andersen[†]
[*]MAN Energy Solutions, Frederikshavn/Denmark,
[†]Technical University of Denmark (DTU), Kgs. Lyngby/Denmark
keun.shin@man-es.com

1 Introduction

Accurate predictions of propeller-induced pressure pulses in cavitating flows are important, because maximum allowable pressure pulses on the hull surface above the propeller are often specified as a requirement for the propeller design and pressure pulse levels are increased 5 to 15 times in cavitating flows relative to without cavitation (ITTC 1999). CFD made by a viscous flow solver is generally known to show higher accuracy and robustness in predicting cavity extents and pressure pulses than potential flow methods (Perali et al 2016). CFD is heavier in terms of computational effort and CFD predictions can be quantitatively varied depending on the numerical setup and cavitation model. Therefore, it is necessary to develop a CFD setup by validating it against experimental results for reliable predictions in cavity extents and pressure pulses.

In this work, CFD simulations are made on INSEAN E779A propeller in the behind-hull condition by a DES solver with a cavitation model and it is validated against experimental results with respect to cavity extents and pressure pulses. The cavitating flows on the target propeller have been considered for validating CFD methods by a number of research groups (Vaz et al. 2015), because a comprehensive series of cavitation tunnel tests have been conducted with measuring cavity extents, pressure pulses and acoustic noise in the open-water and behind-hull conditions (Pereira et al 2004, Salvatore 2006).

As high-frequency oscillations in the pressure field can be numerically generated by low grid resolutions at the interface of the rotating domain and insufficient iterative convergence, the influences of time-step, number of inner iterations and grid size at the interface of the rotating domain on CFD results are investigated by varying these numerical parameters.

2 CFD setup

A DES solver with the curvature-corrected k-ω SST turbulence model in the commercial CFD software StarCCM+ is adopted for unsteady cavitation simulations. Two-phase flows are modelled by the volume-of-fluid (VOF) method and a generic transport equation for vapor volume fraction α_V. Cavitation is modelled by the interphase mass transfer model of Schnerr & Sauer (2001).

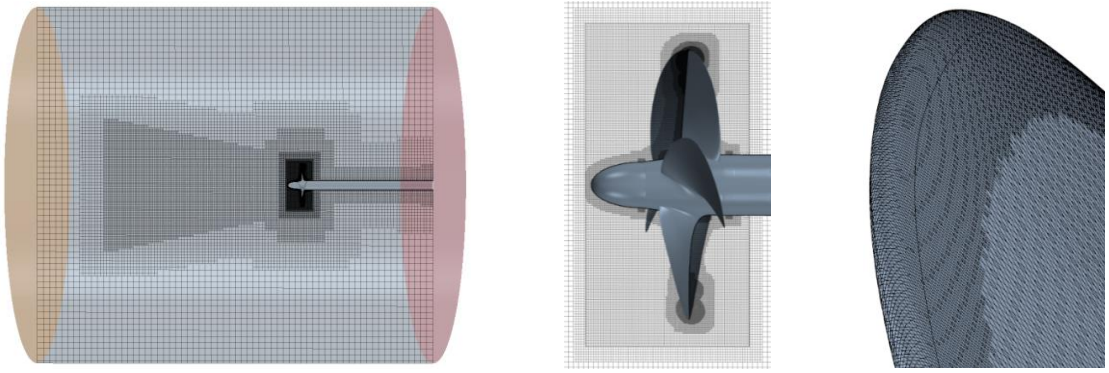

(a) (b) (c)

Fig. 1: (a) Computational domain with the grid on the vertical section, (b) inner rotating domain around the propeller model and (c) surface grid on the blade tip

A trimmed hexahedral grid is generated around the propeller model in a cylindrical fluid domain extending axially 3·D to the inlet, 6·D to the outlet and radially 4·D to the outer wall from the intersection of the shaft axis and the propeller plane, as shown in Fig. 1(a), where D is the model propeller diameter of 227.3 mm. The cross-section area of the computational domain is much larger than that of the cavitation tunnel, so the blockage effect of the cavitation tunnel is neglected in CFD. Instead of simulating the blockage effect, the inflow speed U_O is adjusted to reach the measured thrust in the experiment. The propeller speed is fixed to N = 30.5 rps. Propeller rotations are modelled by the rigid body motion and the sliding grid in a sub-domain around the propeller model, as shown in Fig. 1(b).

The grid size is Δx = 0.2 – 0.5 mm on the blade surface and it is refined to half of Δx at the blade edges, as shown in Fig. 1(c). The grid at the wall boundary has 12 prism layers leading to mostly $y+ \leq 1$. The outer-radius region has a consistent volume grid size of 0.3 – 0.4 mm for resolving cavitating flows better.

While an array of plates are installed to generate hull wake in the upper propeller disk in the cavitation tunnel test, the hull wake measured 0.26·D upstream from the propeller plane is applied to the inlet boundary. The hull wake field is examined by a numerical test in the computational domain excluding the propeller. In Fig. 2, the comparison of the measurement and the wake field of the numerical test shows that the hull wake is well preserved from the inlet to the propeller plane without significant numerical diffusion.

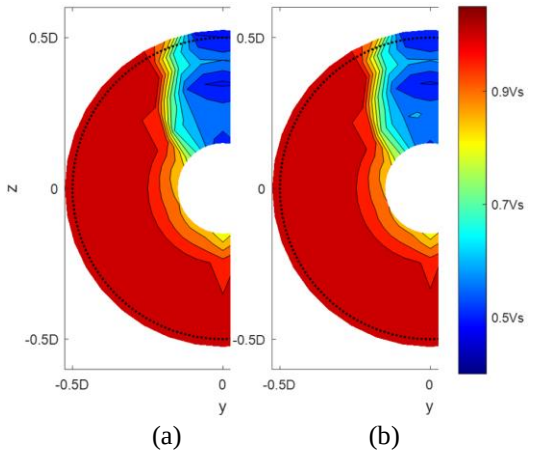

(a) (b)

Fig. 2: Hull wake 0.26·D upstream from the propeller plane without the propeller model – (a) measurements, (b) numerical test

CFD has been validated for fully-wetted and cavitating flows on E779A propeller in the open-water condition (Shin & Andersen 2019) and the validation has shown overestimations of the cavity extent in low cavitation numbers, which are common in other CFD validations made by a number of institutes (Vaz et al. 2015). While a model for transitional flows is included for the open-water condition, it is not included in the current setup for the behind-hull condition.

3 CFD result

CFD is made first at a cavitation number of σ = 10.0 to have the fully-wetted condition, where $\sigma = (P_O – P_V)/(0.5 \cdot \rho \cdot U_{O,Exp}^2)$ and $U_{O,Exp}$ is the inflow speed in the experiment, $U_{O,Exp}$ = 6.22 m/s for the considered advance ratio of J = 0.897. U_O in CFD is iteratively adjusted to reach the measured thrust of K_T = 0.175 within 0.5% deviation. As K_T in CFD at $U_O = U_{O,Exp}$ is 8.3% lower than the measured value, U_O is reduced by 3.2% from $U_{O,Exp}$.

CFD is made at σ = 2.5, which is the lowest cavitation number among those considered in the experiment. The initial simulation is made at a time-step corresponding to $\Delta\theta$ = 0.5° propeller rotation per Δt. CFD is repeated with smaller time-steps of $\Delta\theta$ = 0.25°, 0.125°. A 2nd-order implicit time-stepping scheme is used. CFD is also made with different numbers of inner iterations of N_{Iter} = 5, 10, 20 at $\Delta\theta$ = 0.5°. The surface grid size on the interface of the inner rotating domain is varied in Δx_{Rot} =

2.5, 5, 10, 20 mm to examine the influence of Δx_{Rot} on pressure pulses. Δx_{Rot} = 5 mm is applied to the CFD investigations with varying Δt and N_{Iter}.

3.1 Cavity extent

In Fig. 3, cavity extents in CFD and experimental results are compared. In CFD, cavitation interfaces defined by the iso-surfaces of α_V = 0.1 and 0.5 are in light blue and dark blue, respectively. The blue color at the aft end of the sheet cavity is even darker, as the cavity detached from the blade surface is rolled back by re-entrant jet and so the interface is overlapped. The darker blue part in CFD corresponds to the frothy cavitation at the aft end of the sheet cavity in the experiment.

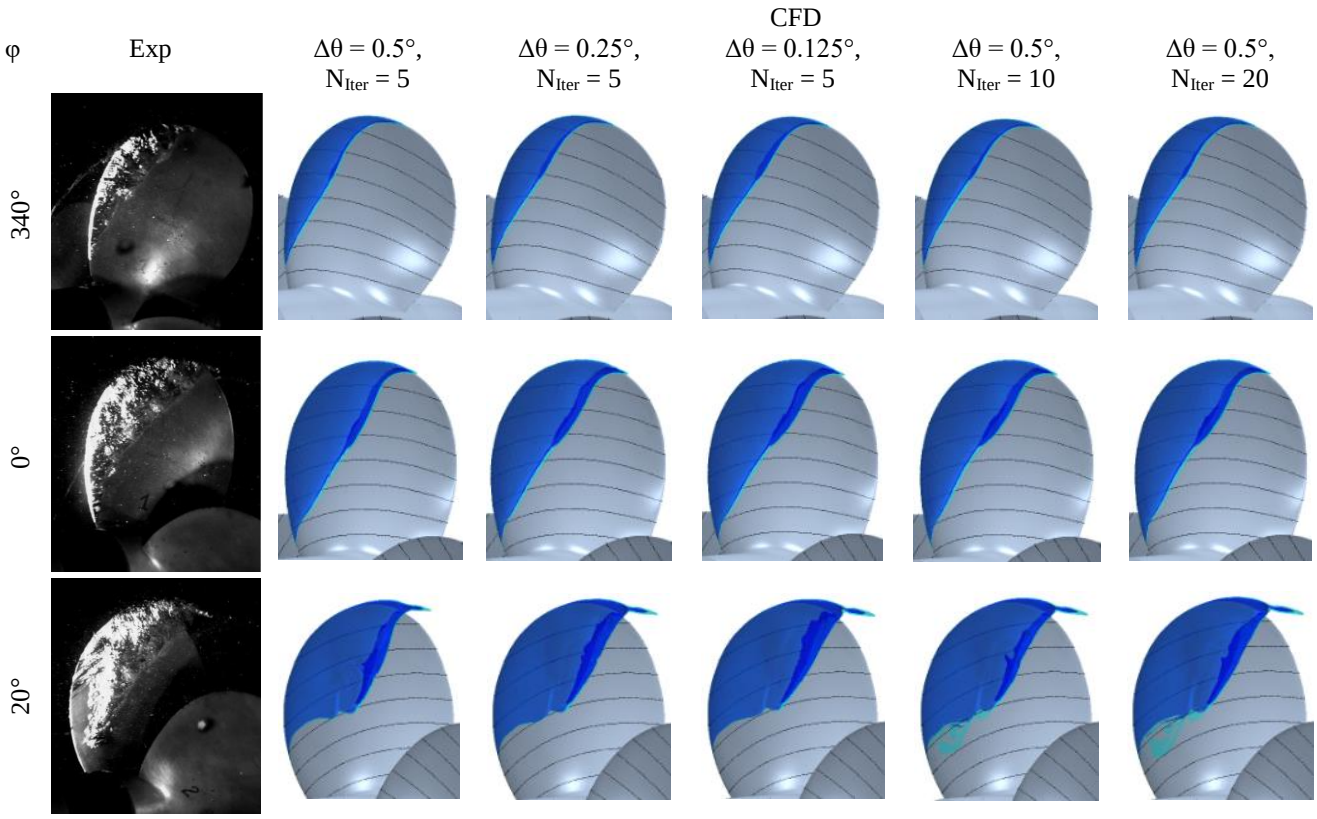

Fig. 3: Cavity extents in the experiment and CFD
(dark blue – α_V = 0.5, light blue – α_V = 0.1)

CFD shows a reasonable agreement in the sheet cavity extent at φ = 340° and 0° with a little underprediction at the outer radii of r/R ≥ 0.8, but the mid-chord cavitation at r/R = 0.45 – 0.7 is not reproduced well at φ = 20° probably due to the fluctuating flows from the wake generator, of which the averaged wake is applied to CFD. The overall sheet cavity is more extended for smaller time-steps and higher numbers of inner iterations. It indicates that the cavity growth is numerically delayed in the initial setup with $\Delta\theta$ = 0.5° and N_{Iter} = 5.

CFD at φ = 20° shows that the sheet cavity at r/R = 0.6 – 0.7 starts from the leading edge regardless of $\Delta\theta$ and N_{Iter}, and scattered cavities with low vapor fractions are formed at r/R = 0.5 – 0.6 for N_{Iter} = 10 and 20. The root mean squared values of normalized residuals for continuity, momentum and turbulence equations are in the order of 10^{-4} – 10^{-6} for N_{Iter} = 5 and those for continuity and momentum equations are reduced to be in the order of 10^{-5} – 10^{-6} for $N_{Iter} \geq 10$.

K_T in the cavitating condition of σ = 2.5 is 1.4% higher than that in the fully-wetted condition. K_T for $\Delta\theta$ = 0.25°, 0.125° and N_{Iter} = 10, 20 is slightly lowered from that in the initial setup, but the

variations are within 0.4%. While the variation of single-blade thrust in Fig. 5(a) shows no noticeable difference except the declining phase, the growing and decaying rates of the cavity are increased for $\Delta\theta \leq 0.25°$ and $N_{Iter} \geq 10$ and so the maximum value of A_{Cav} is increased from 37.5% to 39.6 – 40.3% in Fig. 5(b), where A_{Cav} is the ratio of the surface area under cavity of $\alpha_V \geq 0.1$ to the suction-side blade area.

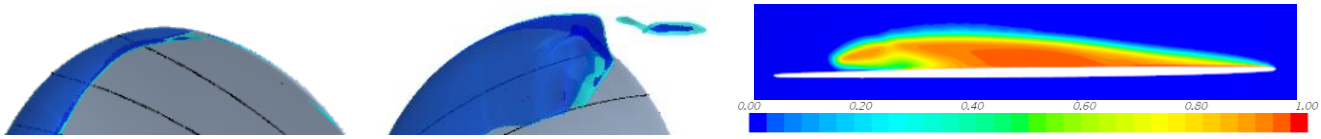

(a) (b) (c)

Fig. 4: Cavity extents at (a) φ = -34° and (b) 42° and (c) α_V at 0.9R section of φ = 15° in CFD

A_{Cav} in CFD is considerably lower than the experimental measurement based on projected areas, firstly because the cavity detached from the surface at the rear part of the sheet cavity is not included in CFD, as shown in Fig. 4(c). The maximum cavity area is shown at $\varphi \approx 15°$, which is later than $\varphi \approx$ -10° showing the maximum $K_{T,1\text{-Blade}}$, as the expansion of the leading-edge cavitation over the chord length takes time. The fluctuations of $K_{T,1\text{-Blade}}$ at φ = -40 – -30° and 30 – 40°, seemingly related to cavitation detachment at the leading edge and trailing edge in Fig. 4(a) & (b), respectively, are alleviated for N_{Iter} = 10 and 20.

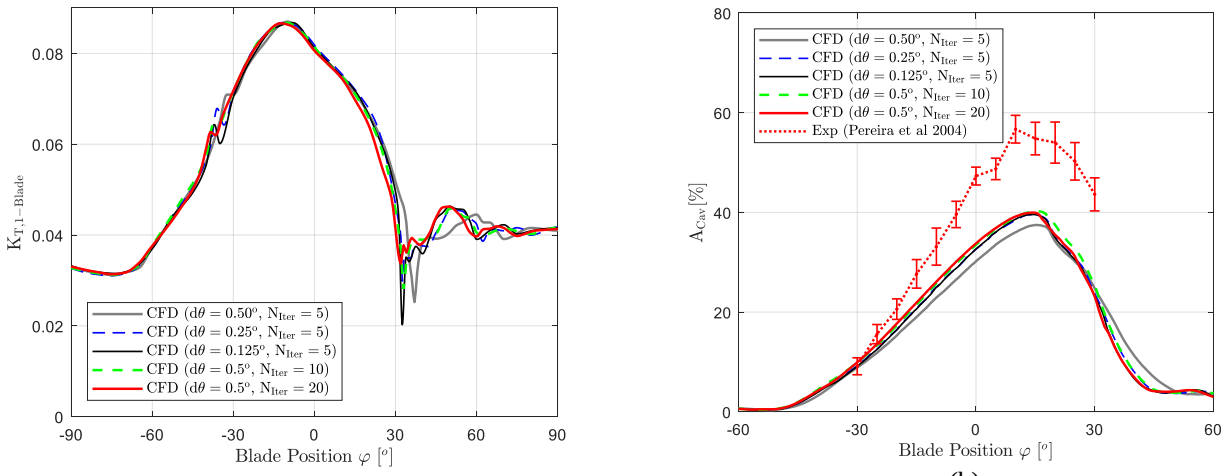

(a) (b)

Fig. 5: (a) Variations of single-blade thrust and (b) cavity area ratio with respect to blade position

3.2 Pressure pulse

In Fig. 6, the comparison of pressure variations on 4 points, which are 0.3 m straightly to the right, above, to the left and below the propeller disk centre (Pereira et al 2004), shows that the peak-to-peak amplitudes on P1 and P4 are overestimated by CFD, whereas the high-frequency fluctuations on P2 are not reproduced and the negative amplitudes on P3 are underestimated. The high-order pressure pulses on P2 can be related to the dynamic behavior of detached cavitation and tip vortex cavitation, which is not simulated well probably due to the insufficient grid refinements and the inflow simplified to averaged axial wake without oscillating vortex shedding. The pressure amplitude is slightly larger and the small fluctuations at peaks and troughs are increased for smaller time-steps and higher numbers of inner-iterations.

In Fig. 7, the pressure pulses at harmonics of the blade passing frequency show that the first-order pressure pulse ΔP_1 is overestimated except P3 and the high-order pressure pulses are underestimated

by CFD. Since pressure variations are probed in the middle of the fluid domain without a wall boundary in CFD, the overestimation of the first-order pressure pulse can be even larger when considering a solid boundary factor of 1.8 – 2.0 (Carlton 2007).

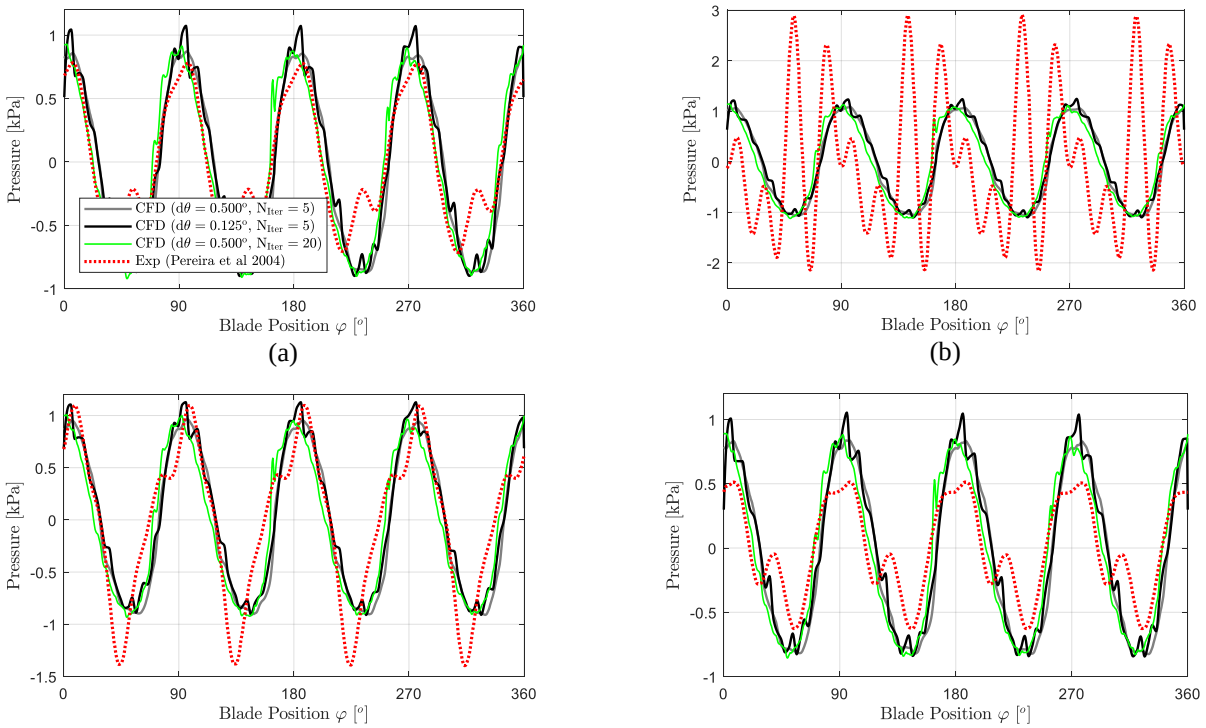

Fig. 6: Variations of pressure on 4 Points – (a) P1, (b) P2, (c) P3, (d) P4

Although P2 is above the upright blade position showing the largest cavitation extent, ΔP_1 on P3 is higher than on P2 in the experiment due to ΔP_3 and ΔP_4 on P2 higher than ΔP_1, whereas ΔP_1 on P2 is the highest among the 4 points in CFD due to the underestimation of high-order pressure pulses.

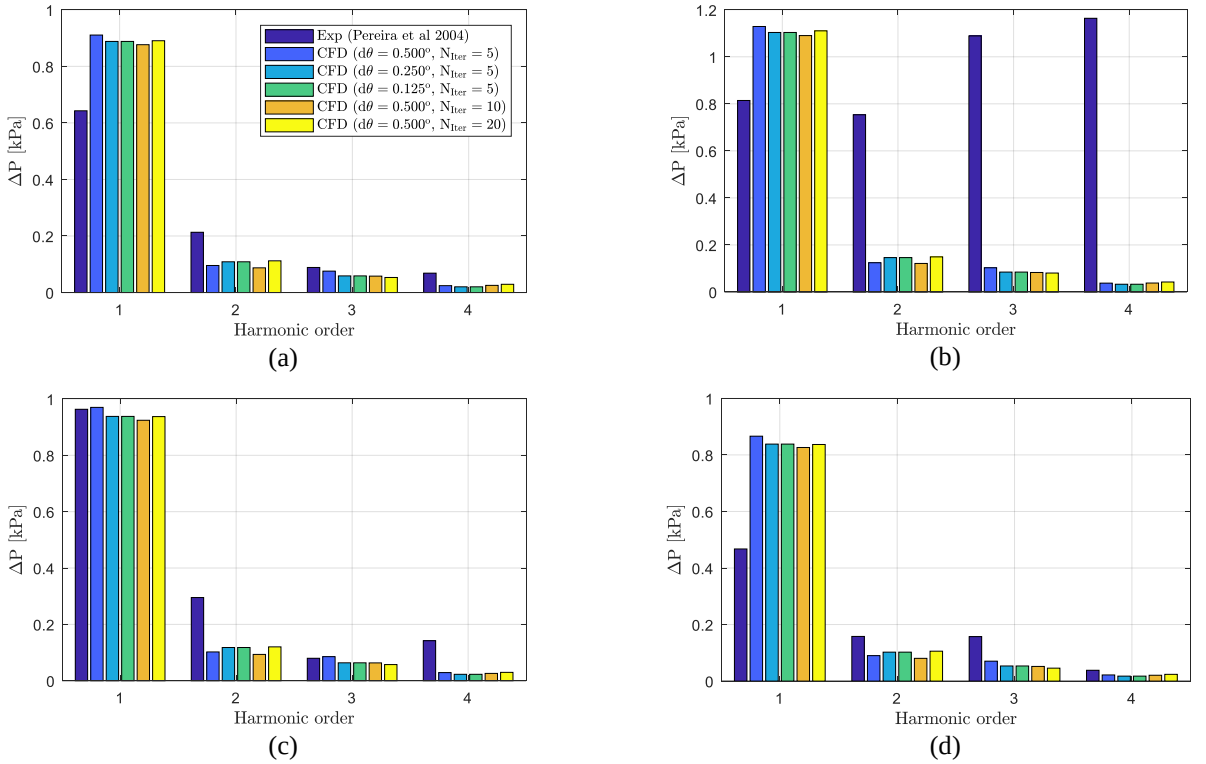

Fig. 7: Pressure pulses at harmonics of the blade passing frequency – (a) P1, (b) P2, (c) P3, (d) P4

While ΔP_1 on P3 is lowered by about 50% on P4 in the experiment, the variation of ΔP_1 at the different points is about 20% in CFD. In CFD, ΔP_1 is lowered by 2 – 5% for $\Delta\theta$ = 0.25°, 0.125° and N_{Iter} = 10, 20, and ΔP_2 is increased by 14 – 20% for $\Delta\theta$ = 0.25°, 0.125° and N_{Iter} = 20, compared to the initial setup. Such changes are still much smaller than the deviations from the experimental result.

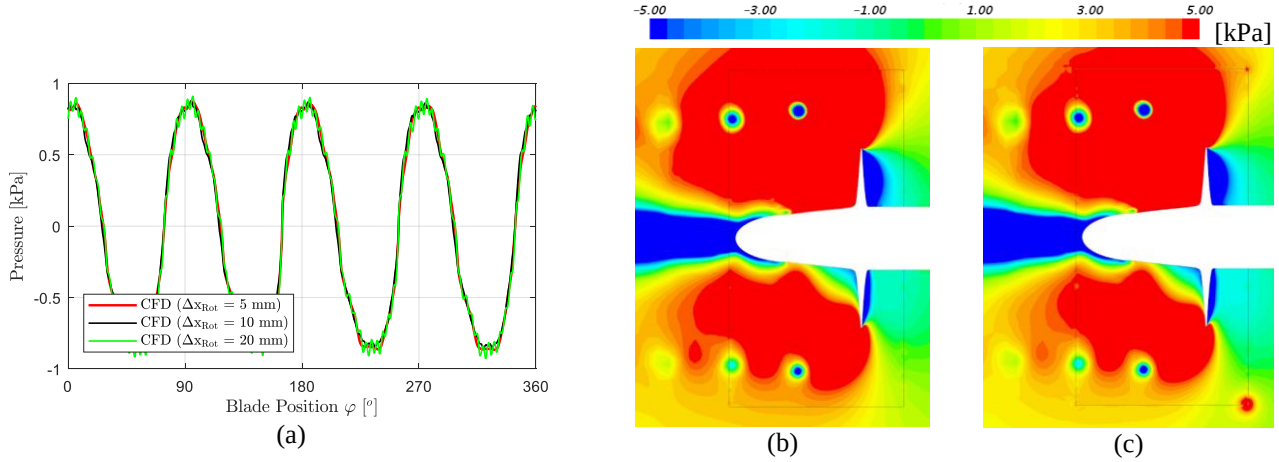

Fig. 8: (a) Pressure variation on P1 in CFD with different values of Δx_{Rot} and pressure distribution on vertical section – (b) Δx_{Rot} = 5 mm, (c) Δx_{Rot} = 10 mm

When Δx_{Rot} is increased to 10 and 20 mm, small oscillations are formed especially at the peaks and troughs of the pressure variation in Fig. 8(a). The pressure fluctuations at the edges of the rotating domain interface are intensified for Δx_{Rot} = 10 mm in Fig. 8(c), which may cause the numerical oscillations of the pressure variations. As the pressure variation in CFD with Δx_{Rot} = 2.5 mm does not show significant differences from that with Δx_{Rot} = 5 mm, $\Delta x_{Rot} \leq$ 5 mm seems sufficient for avoiding numerical pressure oscillations from the interface grid of the rotating domain.

4 Conclusion

The extent of sheet cavity can be underestimated by CFD with insufficient time-step sizes and numbers of inner iterations. The number of inner iterations is important for simulating sporadic cavitation with low vapor volume fractions. Sufficient temporal discretization and numbers of inner iterations can contribute to more accurate predictions of high-order pressure pulses by resolving cavitation dynamics better. Numerical pressure fluctuations can be generated by insufficient grid sizes on the interface of the rotating domain.

References

J.S. Carlton (2007). *Marine propellers and propulsion*. Elsevier

ITTC (1999). The specialist committee on cavitatin induced pressure fluctuation: Final report and recommendations to the 22nd ITTC. Proceedings Of the 22nd ITTC, Seoul/Shanghai, Korea/China

P. Perali, T. Lloyd & G. Vaz (2016). Comparison of uRANS and BEM-BEM for propeller pressure pulse prediction: E779A propeller in a cavitation tunnel. Proceedings of 9th NuTTS, St. Pierre d'Oleron, France

F. Pereira, F. Salvatore, F. Di Felice & M. Soave (2004). Experiment Investigation of a cavitating propeller in non-uniform inflow. Proceedings of 25th Symposium on Naval Hydrodynamics, St. John's, Newfoundland, Canada

F. Salvatore (2006). The INSEAN E779A Propeller Dataset. INSEAN Technical Report, Rome: INSEAN

G.H. Schnerr & J. Sauer (2001). Physical and numerical modeling of unsteady cavitation dynamics. Proceedings of 4th International Conference on Multiphase Flow (ICMF2001), New Orleans, LA, USA

K.W. Shin & P. Andersen (2019). CFD analysis of ship propeller thrust breakdown. Proceedings of 6th International Symposium on Marine Propulsors (SMP'19), Rome, Italy

G. Vaz, D. Hally, T. Huuva, N. Bulten, P. Muller, P. Becchi, J.L.R. Herrer, S. Whitworth, R. Mace & A. Korsstrom (2015). Cavitating flow calculations for the E779A propeller in open water and behind conditions. Proceedings of 4th International Symposium on Marine Propulsors (SMP'15), Austin, TX, USA